3D SPH Simulation of Dynamic Water Surface and its Interaction with Underlying Flow Structure for Turbulent Open Channel Flows over Rough Beds

Eslam Gabreil, Lecturer in Water Engineering, Department of Civil Engineering, Al-Jabal Al-Gharbi University, Gharian, Libya, Email: eslamgabreil@yahoo.com

Simon Tait, Professor of Water Engineering, Department of Civil Engineering, University of Sheffield, Sheffield S1 3JD, UK, Email: s.tait@sheffield.ac.uk

Andrew Nichols, Lecturer in Water Engineering, Department of Civil and Structural Engineering, University of Sheffield, Sheffield S1 3JD, UK, Email: a.nichols@sheffield.ac.uk

Giulio Dolcetti, Research Associate, Department of Civil and Structural Engineering, University of Sheffield, Sheffield S1 3JD, UK, Email. g.dolcetti@sheffield.ac.uk

Abstract

In this study a fully 3D numerical model based on the Smoothed Particle Hydrodynamics (SPH) approach has been developed to simulate turbulent open channel flows over a fixed rough bed. The model focuses on the study of dynamic free surface behaviour as well as its interaction with underlying flow structures near the rough bed. The model is improved from the open source code SPHysics (http://www.sphysics.org) by adding more advanced turbulence and rough bed treatment schemes. A modified sub-particle-scale (SPS) eddy viscosity model is proposed to reflect the turbulence transfer mechanisms and a modified drag force equation is included into the momentum equations to account for the existence of roughness elements on the bed as well as on the sidewalls. The computed results of variousfree surface patterns have been compared with the laboratory measurements of the fluctuating water surface elevations in the streamwise and spanwise directions of a rectangular open channel flow under a range of flow conditions. The comparison has demonstrated that the proposed 3D SPH model can simulate well the complex free surface flows over a fixed rough bed.

Keywords: SPHysics; free surface flow; rough bed; flow surface dynamics; underlying flow structure; flow turbulence; bed drag

1. Literature Review on Dynamic Water Surface Patterns in Turbulent Open Channel Flow

Flows with a free surface in civil engineering applications are mainly turbulent. These include flows in man-made channels and rivers. The study of turbulent flow structures for flows with a free surface is essential to understanding the fluid dynamics for such civil engineering applications. All turbulent flow structures in the natural environment are inherently three-dimensional (3D). These types of flow are characterised by turbulent structures at a range of scales, intense energy dissipation, and random vorticity [Mathieu and Scot, 2000].

When a fluid flows over a solid boundary, the fluid-air interface is often observed to be wrinkled. In open channel flows with the absence of the wind, the vertical velocities must dissipate at the surface, generating horizontal velocities and deforming the surface. Furthermore, turbulent eddies can never die inside the flow; they must end perpendicularly at the free surface, causing temporal changes in water surface elevation above these vortices [Smolentsev and Miraghaie, 2005; Savelsberg and Van de Water, 2009]. Studies of the dynamic behaviour of water surfaces requires the measurement of the instantaneous elevations of the water surface and the instantaneous velocities of the underlying flow. Several techniques have been used to provide a means of measuring these instantaneously and synchronously [Dabiri, 2003; Savelsberg and Van de Water, 2006; Cooper et al, 2006; Nichols et al, 2010; Nichols et al, 2016]. Horoshenkov et al. [2013] measured the instantaneous water surface elevations in turbulent open channel flows using conductance wave probes. The advantage of using conductance wave probes is that, they are easy to set up and calibrate compared to the early mentioned techniques. Conductance wave probes can also be operated at different frequencies to avoid mutual interaction between two or more closely spaced probes, and generally provide high dynamic accuracy.

A number of experimental studies have been conducted and reported in the literature on understanding the linkage between the dynamic behaviour of the water surface and the turbulent flow structures underneath it [e.g., Smolentsev&Miraghaie, 2005; Cooper at al., 2006; Savelsberg et al., 2006; Savelsberg & Van de Water, 2009; Fujita et al., 2011; Horoshenkov et al., 2013; Krynkin et al., 2014]. Kumar et al. [1998] performed an experimental investigation of the characteristics of free surface turbulence in horizontal glass channel flow with Reynolds Numbers ranging from 2800 to 8800. Their results indicated that the persistent structure of the water-air interface can be classified into three types: upwellings, downwellings and spiral eddies. Statistical analyses of Dabiri [2003] have shown that the free surface deformation is strongly correlated with the near surface vorticity field with a correlation coefficient of about 0.7 to 0.8. Smolentsev and Miraghaie [2005] performed an experimental study of flow conditions ranging from weak to strong turbulence in very wide open channel having an aspect ratio (flow width/flow depth) higher than 40. They observed that three types of disturbance are always presented on the free surface at the same time: capillary waves, gravity waves and turbulent waves that are generated due to the interactions between the bulk flow and the water surface. The turbulent waves were found by [Smolentsev

and Miraghaie, 2005] to be the most dominant type, having a characteristic size (in the free surface plane)of approximately half the mean flow depth. An interesting feature has also been observed on the free surface is that these turbulent waves have celerity very close to the average flow velocity, while the speed of capillary and gravity waves were different. This feature was also observed by Fujita et al. [2011]and Nicholas [2014] who stated that the water surface waves travel with velocity close to the mean flow velocity. Savelsberg and Van de Water [2009] reported that although there are several appealing relations between subsurface flow field and water surface gradient, the water surface of fully developed turbulent flow exhibits a dynamic behaviour of its own. They attributed this to the large eddies of subsurface turbulent flow exciting random gravity and capillary waves which move in all directions across the water surface. Fujita et al. [2011] showed that there is a correlation between the vertical velocity components and the boil vortices on the surface that are not due to the gravity waves. Horoshenkov et al. [2013] experimentally studied the free surface dynamic behaviour and its interactions with the underlying turbulence of shallow open channel flows over a gravel bed. The temporal change in water surface elevations was measured using conductance wave probes in the centre of the channel at different streamwise positions. They found that the free surface roughness patterns are strongly controlled by bulk flow properties and are not strongly influenced by gravity waves. Horoshenkov et al. [2013] also showed that the free surface roughness patterns can be described by a well-correlated analytical formula and established a number of empirical relationships between the water surface parameters and the corresponding hydraulic parameters. Nichols et al. [2016] determined the free surface profile for several flow conditions by using the LIF technique and showed that the independent surface behaviour noted by [Savelsberg and Van de Water, 2009] was not due to travelling waves, but due to each individual water surface feature oscillating vertically in time as it is carried in space by the bulk flow. It was concluded that this complex behaviour of oscillating surface features, overlapping and out of phase in space and time, is responsible for decorrelating the surface pattern from the turbulence field that generates it. The spatial period of the oscillation was shown to match the characteristic spatial period of the spatial correlation functions of [Horoshenkov et al., 2013], giving a physical explanation for the oscillatory form of spatial correlation function observed.

2. Literature Review on SPH Applications in Open Channel Flows

Numerical simulations are used as a very valuable tool in the field of hydrodynamics and hydraulic engineering to solve complex problems that are impractical to examine experimentally. They also have the advantage of disclosing details of flow structures without the spatial-temporal limitations of laboratory instruments. Thus they can provide an economical and flexible tool to study flows of practical interest. In numerical simulations, the physical governing equations are described by one of two main approaches. The first one is the mesh-based approach in which the fluid domain is decomposed into a fixed grid. Examples of this approach are Finite Volume (FV), Finite element (FE) and Finite difference (FD). However, simulating complex flows with large deformations is limited and difficult with these methods due to the numerical diffusions raised from the advection terms in the Navier-Stokes (N-S) equations [Gotoh and Sakai, 1999]. The second approach is mesh-free, where the fluid domain is decomposed into moving points of space commonly called

"particles". The Finite Points [Onate et al., 1996], Free Mesh [Yagawa and Yamada, 1996], and Moving Particle Semi-implicit (MPS) [Koshizuka et al., 1998] techniques are all examples of mesh-free approaches. Such techniques are inherently well suited for the simulation of flows with complex boundaries. In recent years, the most popular Lagrangian mesh-free method to have been used is Smoothed Particle Hydrodynamics (SPH). Although the SPH method has been widely used in coastal hydrodynamics, using this method for the simulation of open channel flow problems has received little attention, especially for the simulation of turbulent free surface flows over rough beds. The SPH technique, originally formulated by [Gingold and Monaghan, 1977], initially focussed on the provision of solutions to astrophysics problems related to the formation and eventual evolution of galaxies [Li and Liu, 2004]. It finds wide use in solving applied mechanics problems due to its advantage of using a discretization method to approximate a continuum as a set of particles. The most compelling advantage of the application of the SPH method is its inherent ability to use the set of particles to predict the behaviour of highly strained motions without the need for grids or meshes [Violeau, 2012]. Due to its meshless nature, SPH can handle complex solid boundaries and can also define free surface flows without the typical problems of grid-based methods that they need to be coupled with a suitable technique such as volume of fluid (VOF) to capture the air-water interface.

The treatment of inflow and outflow boundaries in SPH is the key for the successful simulation of open channel flow problems. In recent years, different inflow and outflow boundaries have been implemented. For example, Lee et al. [2008] used a periodic open boundary by which the fluid particles that leave the computational domain through the outflow boundary are instantly re-inserted at the inflow boundary, and the fluid particles close to one open lateral boundary interact with the fluid particles close to the complementary open lateral boundary on the other side of the computational domain. However, this boundary treatment is not suitable for applications in which the fluid volume leaving the computational domain does not have the same fluid volume that needs to be generated to enter the computational domain at the same time. In the technique developed by Shakibaeinia and Jin [2010], the fluid particles leaving and entering the computational domain are added to and subtracted from an additional type of particles called 'storage particles' which exist before the inlet and after the outlet of the domain of interest. With the method used by Federico et al. [2012], the desired pressure and velocity conditions are imposed at the inflow region to the inflow particles and water depth time series are determined by increasing or decreasing the number of particles in the vertical direction. Meister et al. [2014] performed the same numerical technique and the analytical solution of the main velocity and the corresponding pressure distribution were initially imposed. Moreover, Tan et al. [2015] performed an incompressible SPH (ISPH) technique to simulate open channel turbulent flows over a smooth bed. The comparisons indicated that the velocity trend in the upper region is quite promising, but the error becomes larger near the channel bed as the flow depth becomes shallower. Kazemi et al. [2017] used similar techniques of Federico et al. [2012] and Tan et al. [2015], but with the difference in that the inflow particle velocities are linked with those of the inner fluid particles, so that the flow is evolved naturally without any prescription of the inflow velocity.

There is quite limited literature on describing the wall roughness in SPH models of free surface open channel flows. This is a key issue since a hydraulically rough surface exists for most practical hydraulic engineering applications. Gotoh and Sakai [1999] treated the bed roughness by incorporating a drag force term into the momentum equation for a plunging wave interaction with porous bed. Khayyer and Gotoh [2010] implemented a similar treatment for dam break flow over a frictional bed. Generally their results of particle snapshots provided a good match with the measured data. Cleary & Prakash [2004] simulated the historical St Francis dam collapse using real topography which was defined by boundary particles with an interpolation length in the range of 10 m for coarse resolution simulations. The predictions were found to be reasonably consistent with the observed flood time scales. Roubtsova and Kahawita [2006] modelled the well-known Vaiont disaster in Italy 1963, where the topography of the valley was treated by particles and imposing the slip boundary condition. Although the slip boundary and water levels were not known with a high precision, the simulated results agreed fairly well with the sequence of events. Dzebo et al. [2014] performed the SPH modelling of dam break flow through a narrow rough valley. The aim of their study was to show the differences between using a hydraulically smooth terrain (where only the roughness coefficient was considered to account for the drag) and a hydraulically rough terrain (where both the roughness coefficient and form drag were considered to account for the drag due to roughness elements). For a hydraulically smooth surface, two coefficients of eddy viscosity were specified; one for particle-particle and another for particle-wall interactions. For a hydraulic rough surface, the terrain roughness was defined by elevating the grid-nodes resulting in pyramid-shaped elements. The computed results were compared both with measurements on a physical model and results obtained from a 2D-FV model. The comparison of the water surface level showed that the SPH results obtained by either way of defining the roughness terrain agreed better with the experimental data than the FV model. More recently, Kazemi et al [2017] and Gabreil et al [2018] treated the bed roughness by including drag force term into the momentum equation to simulate 2D turbulent open channel flows over fixed beds. Their results of velocity and shear stress show a good macth with the measured data.

In mesh free methods, the free surface can be easily and accurately tracked without numerical diffusion. Since no particles exist in the outer zone of the water surface, the density of a fluid particle drops abruptly on the surface. Different techniques have been developed in the SPH literature to handle this. According to the incompressible SPH (ISPH) approach, the free surface particle is recognized by using the density ratio. A particle is identified as a free surface particle if its density is less than a certain threshold value [Koshizuka et al., 1998; Shao and Lo, 2003]. However, this technique may not be suitable for the weakly compressible SPH (WCSPH) approach noise may exist in the pressure field near the surface. As a result, other researchers have numerically computed the water surface elevations using the Tis Isat model [Petkovšek et al, 2010; Dzebo et al, 2014]. The Tis Isat model calculates water depth at any chosen point using the SPH kernel function. Furthermore, Lee et al. [2008] and Farhadi et al. [2016] used another technique called particle divergence to compute the water surface level. In a 2Dmodel, the divergence is equal to 2.0 when the kernel is fully supported (far enough away from the free surface boundary). Near the water surface the kernel is truncated due to the insufficient number of neighboring particles, and thus the divergence becomes

smaller than 2.0. This feature is implemented to recognize the free surface particles. Lee et al. [2008] and Farhadi et al. [2016] suggested that a threshold criterion ranging from 1.2 to 1.5 can be used to determine which particles belong to the water surface. Most of the free surface particles are accurately detected and some of them could not be detected. This is because the free surface particles that could not be detected have a pressure very close to zero. The defect is acceptable, and it could be further minimized by kernel correction techniques.

In summary, although in the last few decades the SPH modelling technique has been widely used to simulate different free surface flows, very few researchers have used the SPH for the simulation of turbulent open channel flows. Almost no work has ever been reported in the literature of using SPH models to simulate bed roughness in turbulent flows. Additionally, the SPH model has only been used to examine the dynamic behaviour of the water surface in coastal hydrodynamic problems. Therefore, it is important to investigate the capability of this model for simulating free surface turbulent flows over rough beds. In this case, improvements to the 3D SPH turbulence modelling will be made to address the shear stress, and new treatments of rough beds will be developed to account for the form drag forces due to roughness elements. In this study, the improvements made by Gabreil et al [2018] will be extended by taking into account the influence of the 3D flow near the bed and the side walls of the channel. The improved model will then be used to examine the dynamic behaviour of the water surface and its interactions with the underlying flow structures underneath. This work will pave the way to implement the SPH technique in different open channel flows with more complex geometries and rough boundaries, and to extract more details on the flow structure and water surface behaviour, since these details are difficult to obtain using grid-based methods.

This paper is structured as follows. Section 3 covers the 3D numerical model set up and the improvements made on the turbulence model and bed roughness treatment. Section 4 describes the experimental program carried out in a rectangular hydraulic flume with a well-defined rough bed. Instantaneous water surface elevation measurements are reported, including the equipment and calibration processes. Section 5 provides the 3D SPH simulation results with the water surface behaviour being compared with the measured data. Section 6 presents discussion of the findings, the achievements of the work, and recommendations for improvements that could be made on the models to more accurately simulate such free surface flows.

3. Brief Model Review

Implementation of 3D SPH numerical model would allow for more information on the underlying flow structure and water surface pattern to be disclosed, and hence a better understanding on the linkages between the underlying flow and free surface pattern throughout the flow cross section could be addressed.

This section aims to modify the recent 2D SPH code [Gabreil et al., 2018] and make it suitable for 3D free surface flows. Therefore the code will be significantly improved by including a suitable 3D turbulence model to simulate the turbulence transfer mechanisms found over the cross sectional area of a free surface channel flow. A new rough boundary treatment will also be developed based on the concept of drag force model and included code to account for the existence of 3D roughness elements on the channel bed and on both side walls. The numerical results of water surface patterns will be compared to examine whether the improvements made on this model can simulate this type of flow adequately.

3.1 SPHysics code

SPHysics code (http://www.sphysics.org) is a free open-source SPH code that was released in 2007 and developed jointly by researchers at the Johns Hopkins University (U.S.A.), the University of Vigo (Spain), the University of Manchester (U.K.) and the University of Roma La Sapienza (Italy). The code is based on Large Eddy Simulation (LES) and it uses the concept of weakly compressible SPH (WCSPH) to solve the Navier-Stokes equations with different optional add-on features such as boundary treatment, turbulence closure, and viscosity formulation. It is programmed in the FORTRAN language, and has been developed specifically for free surface hydrodynamics [Gómez-Gesteira et al., 2012]. SPHysics code has been used to simulate different phenomena including dam breaks, breaking waves, floating and sliding objects and wave impacts on structures. In this code, a variety of features are available to choose various compiling options and a user manual is also provided. In SPHysics, four different time integration schemes are implemented, i.e. the Predictor-Corrector, Verlet algorithm, Symplectic algorithm and Beeman algorithm. The Predictor-Corrector solution has been mostly used due to its being explicit in time integration and straightforward to implement. Besides, it is also a second-order integration solution, by which the particle velocities, densities, positions, and pressures are computed. To achieve numerical particle stability, a variable time step is controlled by the Courant–Friedrich–Levy (CFL)condition, the forcing term condition, and the viscosity condition [Monaghan, 1992]. In applications of SPH for slightly compressible flows (where the flow pressure is computed by the Equation of State using an artificial sound speed), the fluid particles exhibit large oscillations in the pressure field. Researchers have overcome this problem by performing a filter over the density of fluid particles, normally every 20 to 30 time steps, to smooth out the density and pressure noises. Two different density filter methods are available for users in the SHPysics code. One is called the Shepard filter and the other is the Moving Least Squares (MLS) filter. The advantage posed by the SPH method is that kernels can be calculated through a table or sub-routine. A kernel function defines the width of the influence domain and must satisfy the requirement that it behaves as a delta function as the smoothing length

tends to zero. Thus the dimensional influence of the neighbouring particles is determined. Within SPHysics, the user is able to choose from the available kernel functions. In SPH, the wall boundaries are treated mainly to ensure that fluid particles cannot penetrate the walls, and that the no-slip fluid condition is satisfied. Different wall treatments have been implemented in SPH applications, for example ghost particles, repulsive particles and dynamic particles. In SPHysics, two different choices of solid boundary are available for users; repulsive particles and dynamic particles. The dynamic wall particle treatment is advantageous mainly because of its computational simplicity, since the wall particles are computed inside the same loop as the fluid particles, and thus the computational time is reduced. SPHysics code treats the inflow and outflow boundaries using the periodic open boundary described by Lee et al. [2008].

3.2 Model setup and computational parameters

To be dimensionally consistent with the experiment, the numerical flume width was taken as 0.46 m wide for the four flow conditions listed in Table 1. To provide sufficient numerical accuracy and low CPU load simultaneously, the numerical flume length was considered to be three times the total flow depth as sketched in Figure 3. This length is believed to be sufficient enough to numerically visualize spatial stable patterns of water surface. The initial particle size was selected as 0.0015 m for flow conditions 1 and 2, and 0.0025 m for conditions 5 and 8, respectively. This provides a range of 80,0000 ~ 98,0000 particles involved in the computation domain. The selection of particle size is to ensure enough resolution within the bed roughness elements and also to minimize the kernel truncation near the boundaries. Similar to 2D model [Gabreil et al., 2018], a cubic spline kernel was adopted with a kernel size of h = 1.5dx. The real water viscosity ($\upsilon_0 = 10^{-6}$ m²/s) was used and the MLS filter was applied every 30 time steps to smooth out the density and pressure fluctuations. The computational time step was automatically adjusted to follow the Courant stability requirement [Gómez-Gesteira et al., 2012]. To reduce the CPU time and meet the requirement for achieving flow stability, a speed of sound c_0 = 20 m/s was used throughout this computation. This value is approximately 3 times larger than the minimum requirement ($c_{0(min)} = 10U_{max}$) as suggested by [Monaghan, 1992]. The XSPH variant was found to result in numerical dissipation and therefore it was turned off. The 3D SPH numerical model was run for flow condition 1, 2, 3, and 4 listed in Table 1 until time t exceeded 6.0 s using an output time of 0.02 s. To reduce the time of simulation and to reach the stable flow quicker, an analytical solution based on the power law $U = U_{max}(y/H)^{(1/m)}$ was initially imposed within the fluid block for each flow condition. It should be noted that nothing has been imposed on the inflow/outflow, bottom and side wall boundaries, instead the turbulent flow has been developed by the influence of the proposed 3D turbulence model and drag force equations demonstrated later. The value of m in the power law equation was determined from the best fit with the experimental time averaged streamwise velocity profiles at the flume centreline as m=2.8, 3.0, 3.2, and 3.8 for flow condition 1, 2, 3 and 4, respectively. It was observed that stable depth averaged streamwise velocity has been achieved at t= 3.0 s after the flow was initialized for the four flow conditions. This allows for 3.0 s of data

gathering that could be said to have no longer been under the influence of the initial model setup. Similar to the previous 2D model [Gabreil et al., 2018], the bed reference level y_0 was taken 4.0 mm below the top of the spheres (the red dashed-line in Figure 1), from which the mean flow depth h_w is measured. In this 3D model, a value of $h_d = 0.32D$ was used for flow conditions 1 and 2 (shallower), and $h_d = 0.24D$ was used for flow conditions 3 and 4 (deeper). This actually makes physical sense in that shallower flow conditions experience proportionately higher flow resistance and therefore need a larger roughness height to generate this higher flow resistance. This also can be observed in the calculated values of the hydraulic roughness k_s listed in Table 1. Since the flow is 3D, it is expected that smaller values of h_d, as compared to those values used in 2D model, can provide a better match with the experimental velocity profiles. This could be attributed to the fact that in a 3D model, the lateral and vertical velocities near the bed and side walls of the channel would also remove some momentum from the flow which is not accounted for in the 2D model. Both $h_d = 0.24D$ and $h_d = 0.32D$ are within the range widely reported in the literature [Nakagawa et al., 1975].
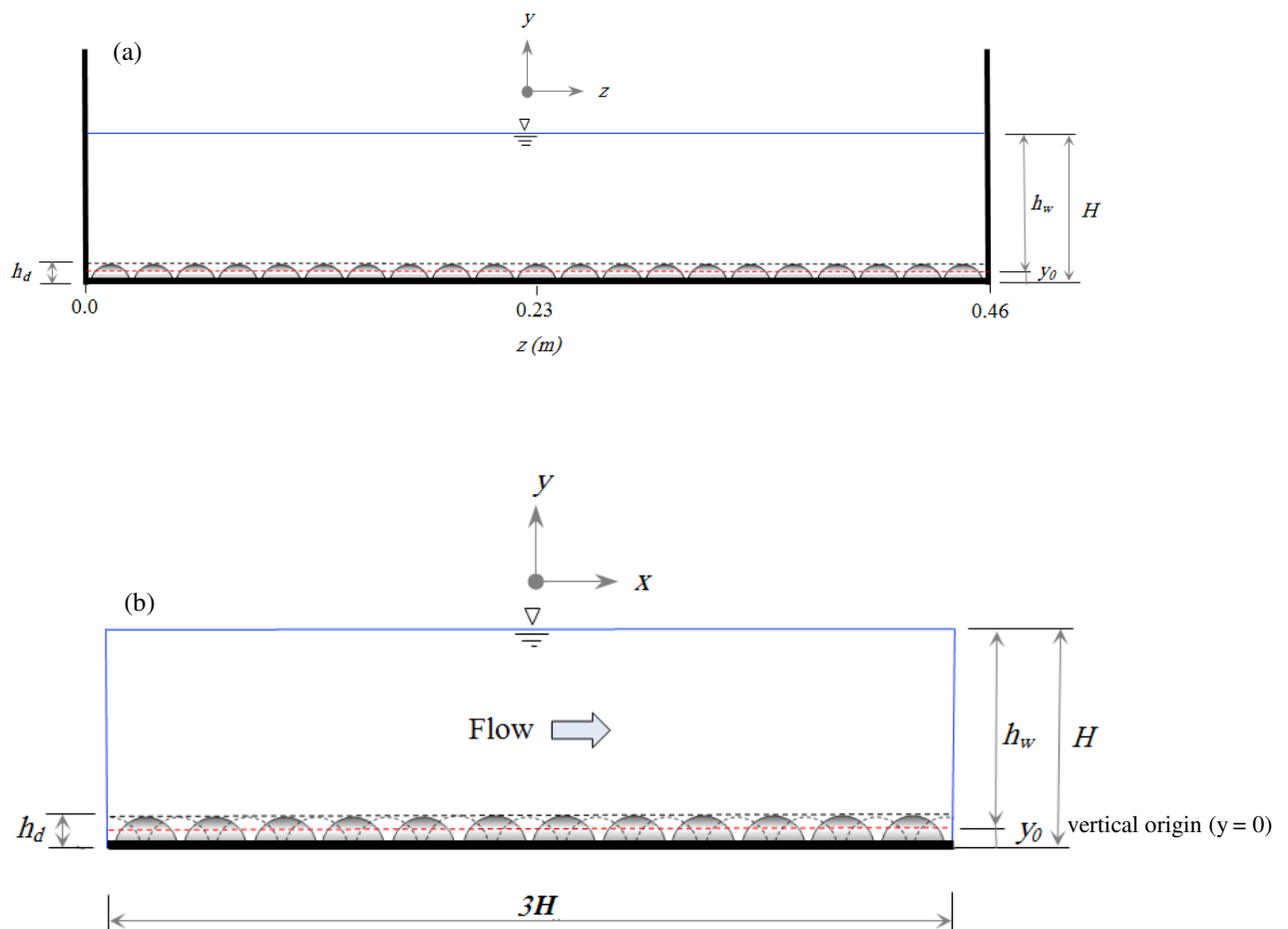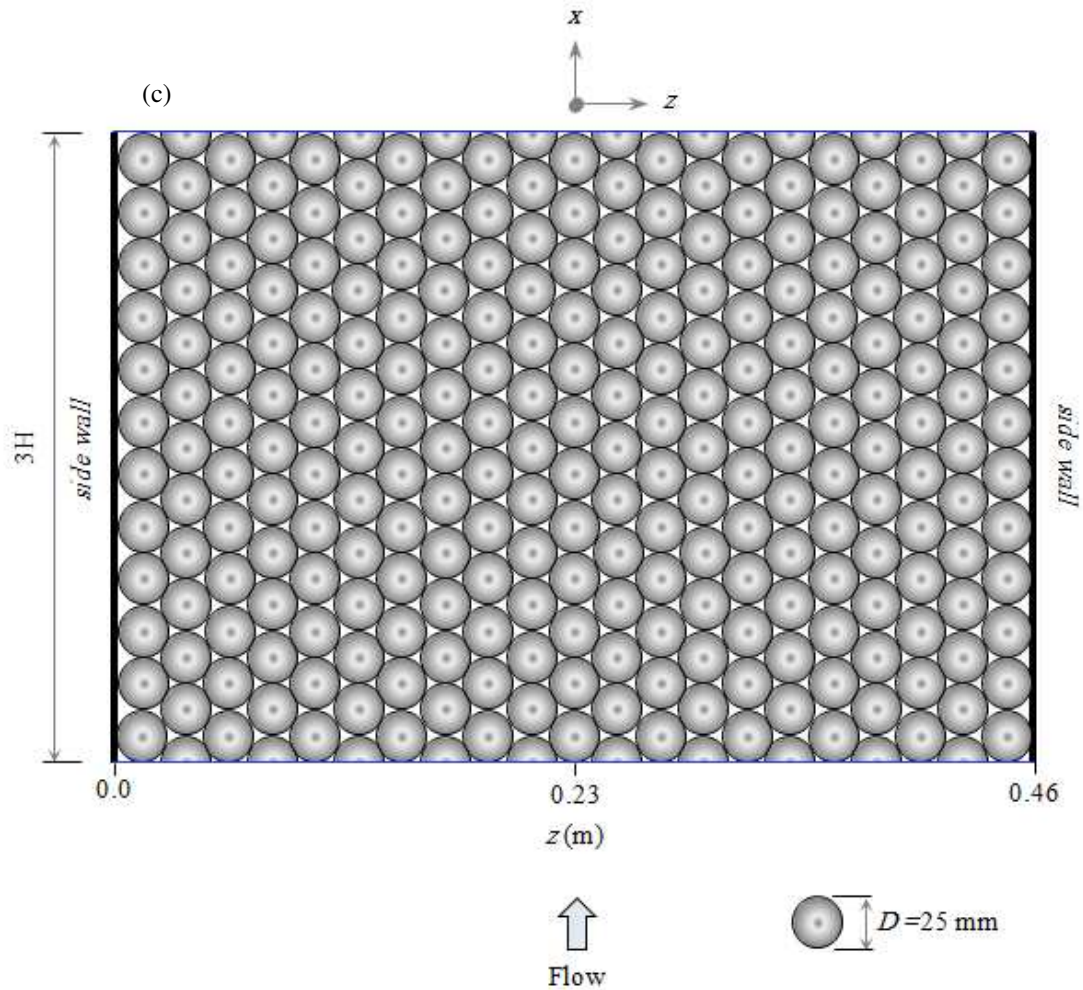
Fig.1. A sketch of 3D numerical model domain including bed roughness elements; (a) cross sectional view; (b) longitudinal view; (c) top view.

3.3 Treatment of turbulence and roughness elements in 3D model

Similar to 2D model of [Gabreil et al,. 2018], the flow turbulence shear stress is modelled by using the eddy viscosity Sub-particle Scale (SPS) model [Gotoh et al., 2001; Lo and Shao, 2002]. In this 3D numerical simulation of free surface flows, it was found that the original SPS turbulent model using fixed Smagorinsky constant provides a much smaller shear stress value as compared with the experimental data. This phenomenon was also observed in the previous 2D SPH model of [Gabreil et al., 2018]. Czernuszenko and Rylov [2000] proposed a simple analytical model based on the generalisation of Prandtl's mixing length approach that could be used to obtain the mean velocity and shear stress distributions in 3D non-homogeneous turbulent flows. This simple model was also implemented in the current 3D SPH model by modifying the original SPS model. That is to say, the fixed product $C_s\Delta$ in the turbulent eddy viscosity was replaced by a mixing length formulation which represent the turbulent eddies scale. For more details on the improved mixing length formulation in 3D, refer to [Gabreil, 2017].

In 3D turbulent open channel flow, the flow is not only influenced by the existence of the roughness element on the channel bed, but it is also influenced by the vertical side walls. This section aims to develop a new treatment of rough boundary to account for the drag forces due to the roughness element on both types of boundary.

To prevent the inner fluid particles from penetrating the bottom and side wall boundaries, the dynamic SPH particles approach [Dalrymple and Knio, 2001] has been implemented. It has been found that this boundary treatment behaves as a hydraulically smooth bed, and it does not adequately exert a frictional effect on the flow. In the present work, the channel bed was covered with hexagonally-organised spheres with a diameter of 25 mm. Such a rough bed can be classified as hydraulically rough, since the hydraulic roughness is independent of the flow Reynolds Number. Therefore, the frictional forces on the channel bed have to be accounted for.

In the current numerical simulation, the bed drag force was quantified using the classic drag formula given in [Gabreil et al., 2018] and added to the momentum equation. It should be noted that, in 3D flow over rough bed the drag force acts in the streamwise, vertical and lateral directions. The lift force was neglected here due to being very small and it is believed to have no significant influence on the flow. The vertical drag forces were only computed on the sidewalls where high vertical velocities occur due to the interaction between the flow and sidewall corners. Following Gabreil [2017], the drag forces acting on the vertical side walls are proportional to those on the channel bed through the shear stress distributions on the different regions of the cross section.

4. Experimental Study

4.1 Aims of the experiments

The aim of these experiments was to measure the temporal change in water surface elevations at different locations in the streamwise and lateral directions. These measurements are then used to support the application of the SPH approach for use in open channel shallow, turbulent free surface flows. This will allow examination of the underlying flow patterns and the water surface spatial pattern.

4.2 Hydraulic flume setup

Measurements were carried out in a 0.459 m wide and 12.6 m long rectangular open channel flume including a recirculating water system. At the upstream end the hydraulic flume is

supported on a fixed pivot joint, and on a pivot joint attached to an adjustable jack at the downstream end. The sidewalls of the flume were composed of glass to enable flow observation. To form a well-defined rough bed surface, the channel bottom was covered by two layers of smooth plastic spheres with diameter of D = 25.0 mm and density of 1400 kg/m³, which were arranged in a hexagonal pattern as shown in Figure 2.
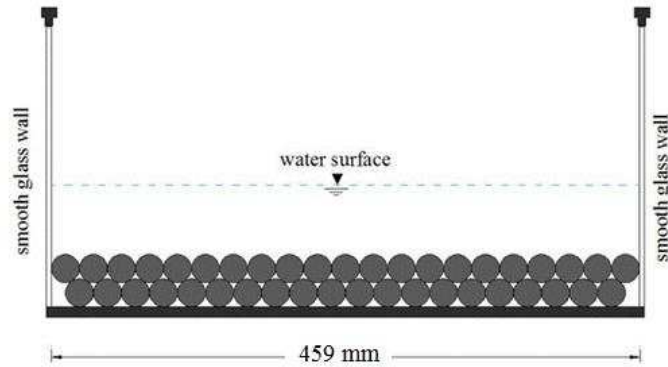

Fig. 2. Cross sectional view of the flume included the spheres

In this study, a number of four hydraulic flow conditions were selected using a range of water depths and bed slopes that would provide a range of Froude Numbers as shown in Table 1, where hydraulic roughness is calculated using the Colebrook-White equation. These flow conditions were selected to investigate the influence of rough bed elements on the water surface patterns of the turbulent flows. The experimental Reynolds Numbers (Re) ranged from approximately 11000 to 43000, so all the flows were fully turbulent.

Table 1. Summary of the experimental flow conditions

Flow condition (-)	Uniform flow depth h_w (mm)	Mean velocity $\overline{U}$ (m/s)	Shear velocity u^* (m/s)	Flow rate Q (m3/s)	Bed slope S_0 (-)	Reynolds Number Re (-)	Froude Number F_r (-)	Hydraulic roughness k_s (mm)
1	40	0.28	0.039	0.008	0.004	11200	0.447	35.0
2	50	0.35	0.044	0.011	0.004	17000	0.499	35.0
3	70	0.36	0.045	0.016	0.003	30800	0.434	30.0
4	100	0.43	0.044	0.023	0.002	43000	0.434	22.0

4.3 Water surface measurement

The temporal changes in the water surface were measured using conductance wave probes. The wave probes consisted of two thin wires, which were laterally separated by a distance of 13.0 mm. For this experiment, a tinned copper wire of 0.25 mm in diameter was adopted in order to minimise any effect on the surface pattern. An array of eight conductance wave

probes (SP1 to SP8) was installed along the flume centreline, starting at 9.0 m from the flume inlet (the black circles in Figure 3), in order to measure the instantaneous free surface elevations at different streamwise locations. Additionally, two lateral arrays of eight conductance wave probes each (the grey circles in Figure 3) were installed in one half of the flume cross section to measure the instantaneous water surface elevations in the lateral direction. The eight probes of the first lateral array are labelled as 1L1 to 1L8, while for the second lateral array are labelled as 2L1 to 2L8 in Fig 3. The two lateral arrays are separated by a streamwise distance of 300 mm to ensure uniformity of free surface measurement. The positions of the streamwise and lateral conductance wave probes were selected in order to obtain unique numbers of spatial separation. At the bottom of the flume, the upper layer of spheres were drilled with 1.0 mm diameter holes, and each probe was carefully attached into these holes. The drilled spheres then were fixed into the bed using strong glue. At the top, each wave probe was connected to a screw system enabling the wire to be vertically held under tension without causing plastic deformation. The overall error in the probe positions between the two lateral arrays was 2.5%. All the probes were connected to wave monitor modules provided by Churchill Controls. For each wave monitor module output, a 10 Hz low-pass filter was used to eliminate high frequency noise. The wave monitor modules provided analogue voltage signals between ±10V, which were tuned to cover flow depths ranging from 30 mm to 130 mm. Each wave monitor module allows a maximum number of eight wave probes to be simultaneously operated. All the installed wave probes were simultaneously calibrated and the process of this calibration was as follows. The flume was set to a slope of $S_0 = 0.0$, and both inlet and outlet ends were carefully blocked to ensure that water cannot leak from the flume. The water in the flume tank was then pumped into the flume until a desired water depth was achieved. When the water in the flume settled down (horizontal water surface) after half an hour, the voltage readings of the wave probes were recorded at 100 Hz for a period of 1800 s by the use of a LabView program. This procedure was repeated for a number of six flow depths ranged from 30 mm to 130 mm, so that a linear trend between the water depth and voltage was achieved for each wave probe. This linear relationship then was used to convert the time-dependent voltage recorded on a wave probe into time-dependent water elevations.
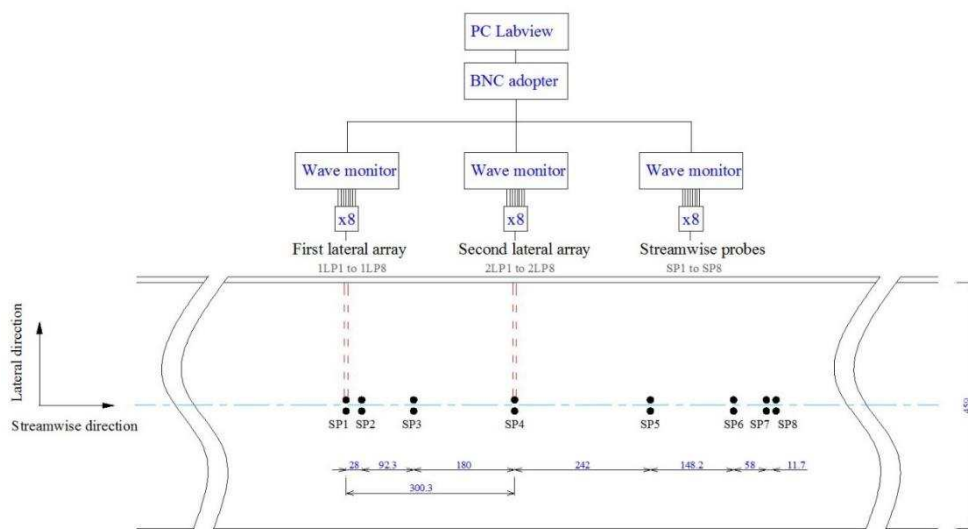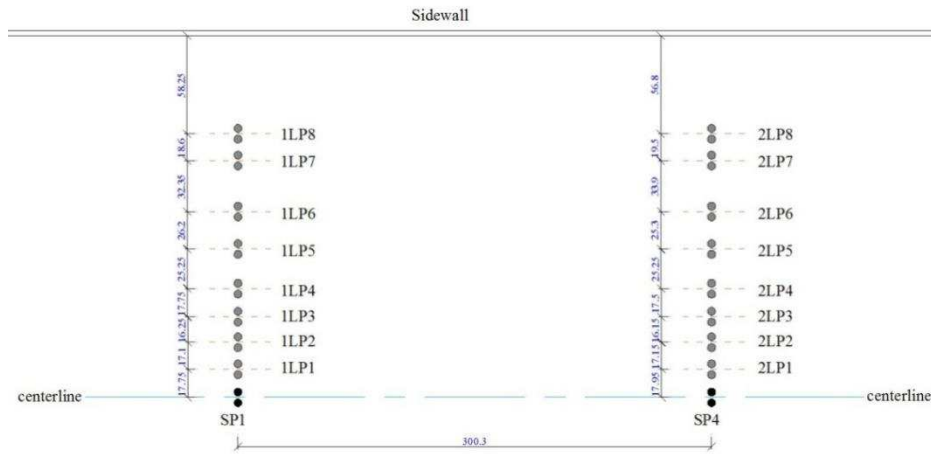
Fig. 3. Top view of laboratory wave probe equipment and position schematics within the measurement section (All dimensions in mm).

4.4 Water surface data collection

Before water surface measurements were taken, the uniform steady flow condition was first achieved and was allowed to stabilise for at least one hour. This is to ensure that accurate temporal water surface behaviour is captured. These measurements were taken for all the examined flow conditions in Table 1. The voltage signals of all probes were recorded at a sampling frequency of 100 Hz and a sampling time of 1800 s. A digital thermometer was used to measure water temperature before and after taking water surface measurements. This is to ensure constant water viscosity throughout the measurements, and to avoid temperature variation effects in the wave probe calibrations. For all flow conditions the water temperature change was within 5.0% of the mean measured value.

Figure 4 shows the Probability Density Function (PDF) obtained for the wave probe signals in all the examined flow conditions. The solid red lines presented in Figure 2 correspond to the best match with a Gaussian function as, $\mathrm{PDF}(\mathrm{h'}_w) = \mathrm{e}^{-(\frac{\mathrm{h'}^2_w}{2\sigma^2})}/\sigma\sqrt{2\pi}$, where $\mathrm{h'}_w$ and σ are the water surface fluctuations and their standard deviation (STD), respectively. It can be seen that the behaviour of the PDF closely follows a Gaussian distribution. The error in σ value obtained from the above Gaussian function and from wave probe statistics remains below 2.0% for the four flow conditions. Also the value of σ was found to increase as the flow depth increases from condition 1 to 4. These observations agree well with the experimental findings

14

reported by [Horoshenkov et al., 2013] and [Nichols et al., 2016] who measured the water surface fluctuations using conductance wave probes and image based Laser Induced Fluorescence (LIF), respectively. The measured data here will be used to support the development of the 3D SPH numerical model which is demonstrated in the following section.
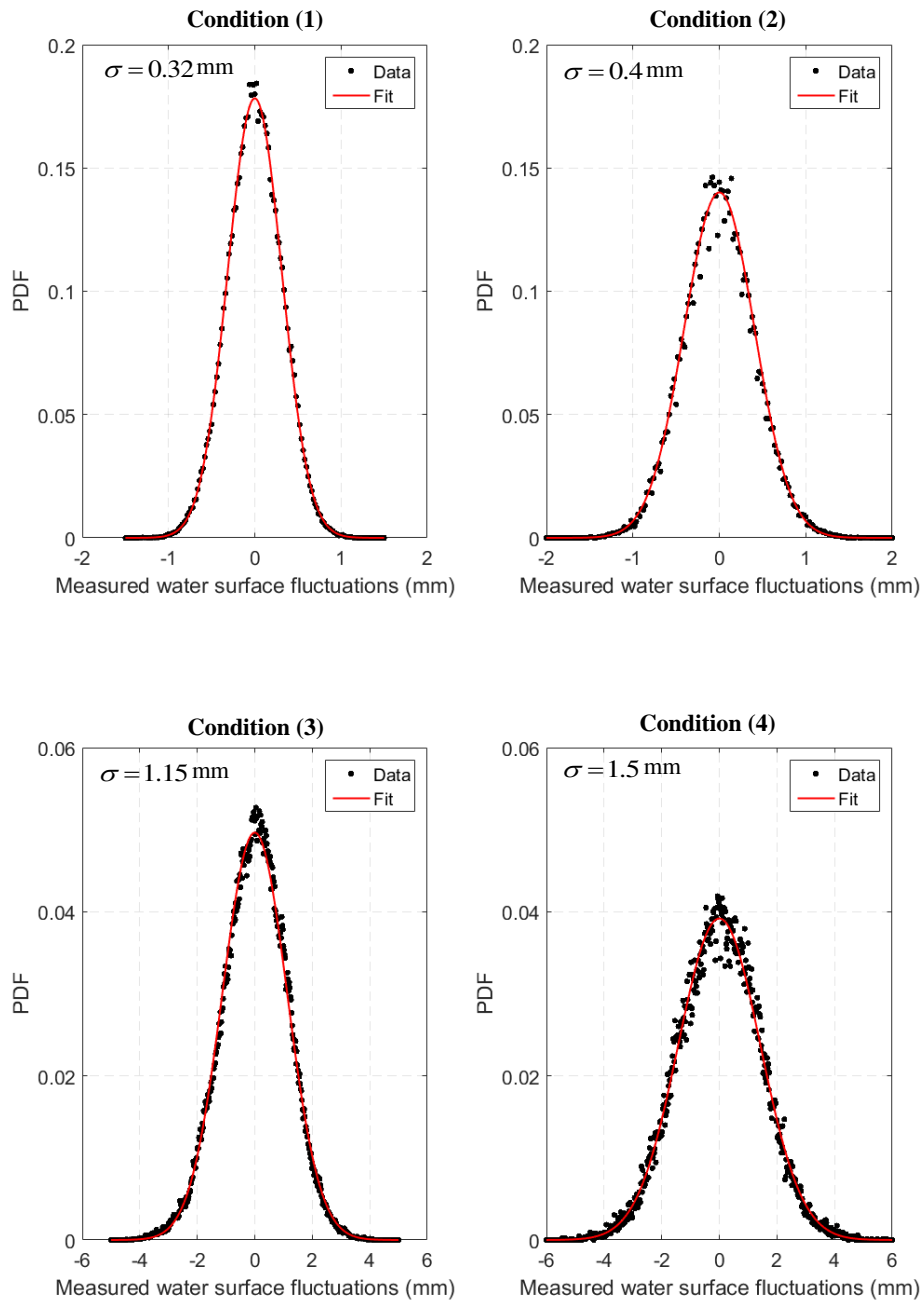

Fig.4. Probability Density Function (PDF) of the measured water surface fluctuations for all flow conditions in Table 1.

5. 3D SPH Model Applications and Results Analyses

This section will examine the newly developed 3D SPH model in predicting the mean flow depth by comparing the predicted data with the experimental observations. The model will also be used to attempt to simulate the dynamic behaviour of the free surface and its interaction with the underlying flow.

5.1 Water surface pattern

Similar to the 2D SPH model, the water surface elevations were extracted from the SPH particle data using the principle of the divergence of particle position [Gabreil et al., 2018]. In the 3D model, it was found that when the kernel is fully supported, the particle divergence $\nabla \cdot \mathbf{r}$ is approximately equal to 3.0. At the free surface a value of $\nabla \cdot \mathbf{r} = 1.5$ was found to give the highest standard deviation of the free surface. Therefore this was used to compute the instantaneous water surface elevations in the streamwise and lateral directions as follows.

The free water surface is divided into mesh-grid points in the streamwise and lateral directions, and these grid points are equally separated by a distance $\Delta x = \Delta z = 5\,\text{mm}$. This gives a total number of 93 grid points along the lateral direction and 25 to 60 grid points in the streamwise directions. At each grid point (x,z), several vertical locations were defined below and above the initial water surface level using a spacing of $\Delta y = 0.01$ mm. The particle divergence $\nabla \cdot \mathbf{r}$ was then computed at each of these locations. The vertical location which corresponds to the value closest to $\nabla \cdot \mathbf{r} = 1.5$ was taken as the instantaneous water surface elevation. This computation was performed over time t = 3.0 s resulting in a total of 3/0.02 = 150 sets of time series.

The probability density function (PDF) of the water surface fluctuations computed by the above procedure is presented in Figure 5 for the four flow conditions. The computed PDF closely follows the Gaussian distribution (the red-solid lines in Figure 5). It is also worth noting that the computed standard deviation σ varies for each flow condition, such that it increases as the flow becomes deeper, which agrees with the experimental observations (see Figure 4). Here it should be noted that the proposed 3D SPH model still predicts the standard deviation of water surface fluctuations smaller than that in the experiments. Also the standard deviation of the water surface fluctuations predicted by 3D model is smaller than that computed from 2D model of [Gabreil et al., 2018]. Since different sound speed values were used for each model ($c_0 = 60$ m/s for 2D model, and $c_0 = 20$ m/s for 3D model), these findings would suggest that the sound speed has an influence on the computed water surface fluctuations.
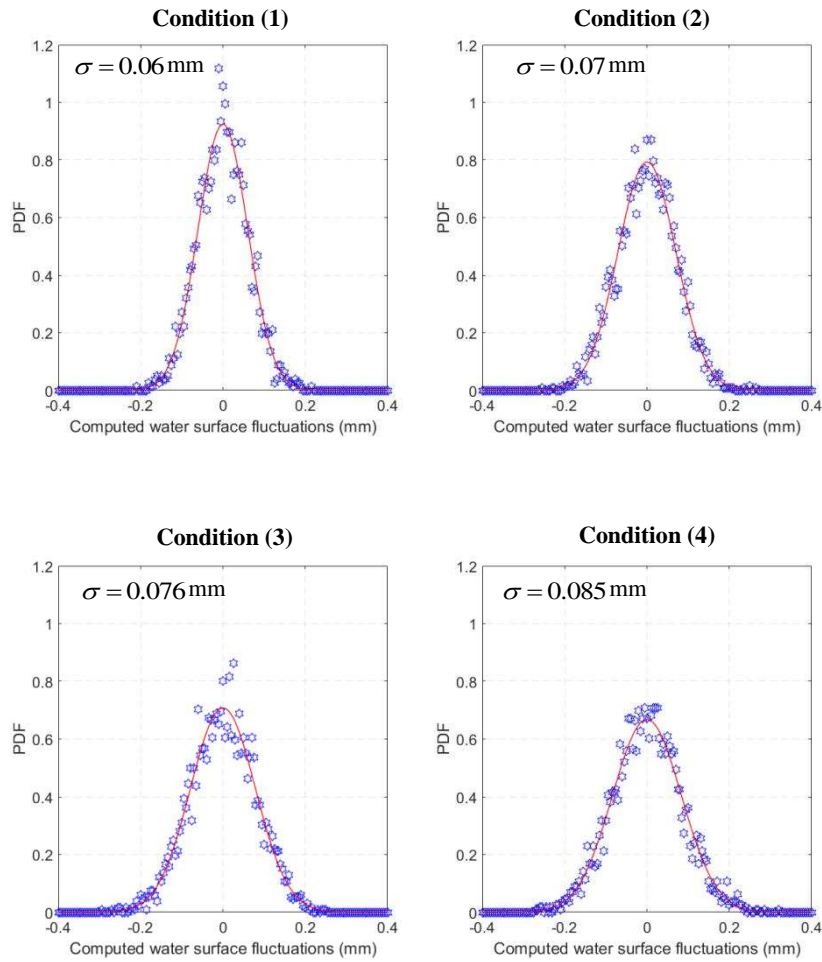
Fig.5. Probability density function (PDF) of the computed water surface elevations for the four flow conditions(blue circles: SPH; and red-solid lines: Gaussian curve).

As far as the author is concerned, the possible reasons as to why the present 3D models were not able to predict larger water surface fluctuations are due to the following reasons. In the current SPH model, the drag force was used to model the rough bed rather than modelling the real roughness geometry. This treatment may have significantly disregarded the flow dispersion throughout the flow depth and hence the effect of this on the water surface fluctuations could not be clearly seen. In SPHysics code which is based on the use of weekly compressible SPH approach, the computed pressure at the free surface is not precisely zero, due to the flow being assumed to be slightly compressed by the use of artificial sound speed. This may influence the results when computing the instantaneous water surface elevations using the particle divergence $\nabla \cdot \mathbf{r}$. Therefore the sound speed value used in the 3D model may have dampened the free surface fluctuations. The use of density filtering operations in the current model to deal with numerical noise may also contribute to this situation. Also it might be possible that in order to predict the water surface fluctuations more accurately, the computational particle size should be much smaller than the experimental water surface fluctuation size and thus the influence of the kernel averaging domain is minimized. Using

smaller computational particle size means that smaller turbulent flow structures are resolved and their influence of the free surface might be observed as well.

5.2 Spatial distribution of the computed mean water level

The time averaged water surface elevations at each grid point were computed and plotted in Figure 6 for the four flow conditions. In the regions very close to the side walls and the inflow and outflow boundaries (where the kernel is truncated due to the insufficient number of neighbouring particles), the computed water elevations were noisy and therefore they were removed from the plots. These contour plots show that the mean water surface elevations are almost symmetrical in both sides of the flume without any significant numerical noise. A lateral variation of the mean water surface elevations can be observed across the flume width. For the four simulated flow conditions, the maximum mean water surface elevations occur in regions close to both sidewalls due to the interaction between the flow and the sidewalls. Far away from both sidewalls, the variation in the mean water surface elevations becomes very small. The difference between the maximum and the minimum free surface elevations among the four conditions remains less than dx (where dx is the initial partial size).

Condition (1)

Condition (2)
$\overline{h}_w$(mm)

Condition (3)
$\overline{h}_w$(mm)
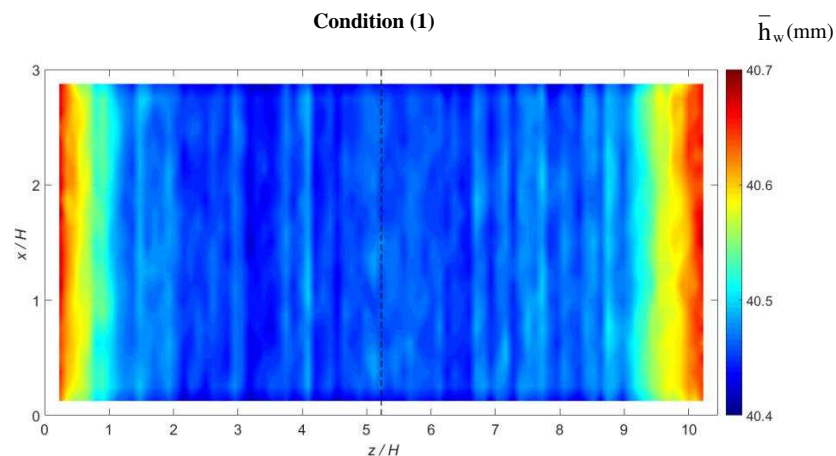
Condition (4)
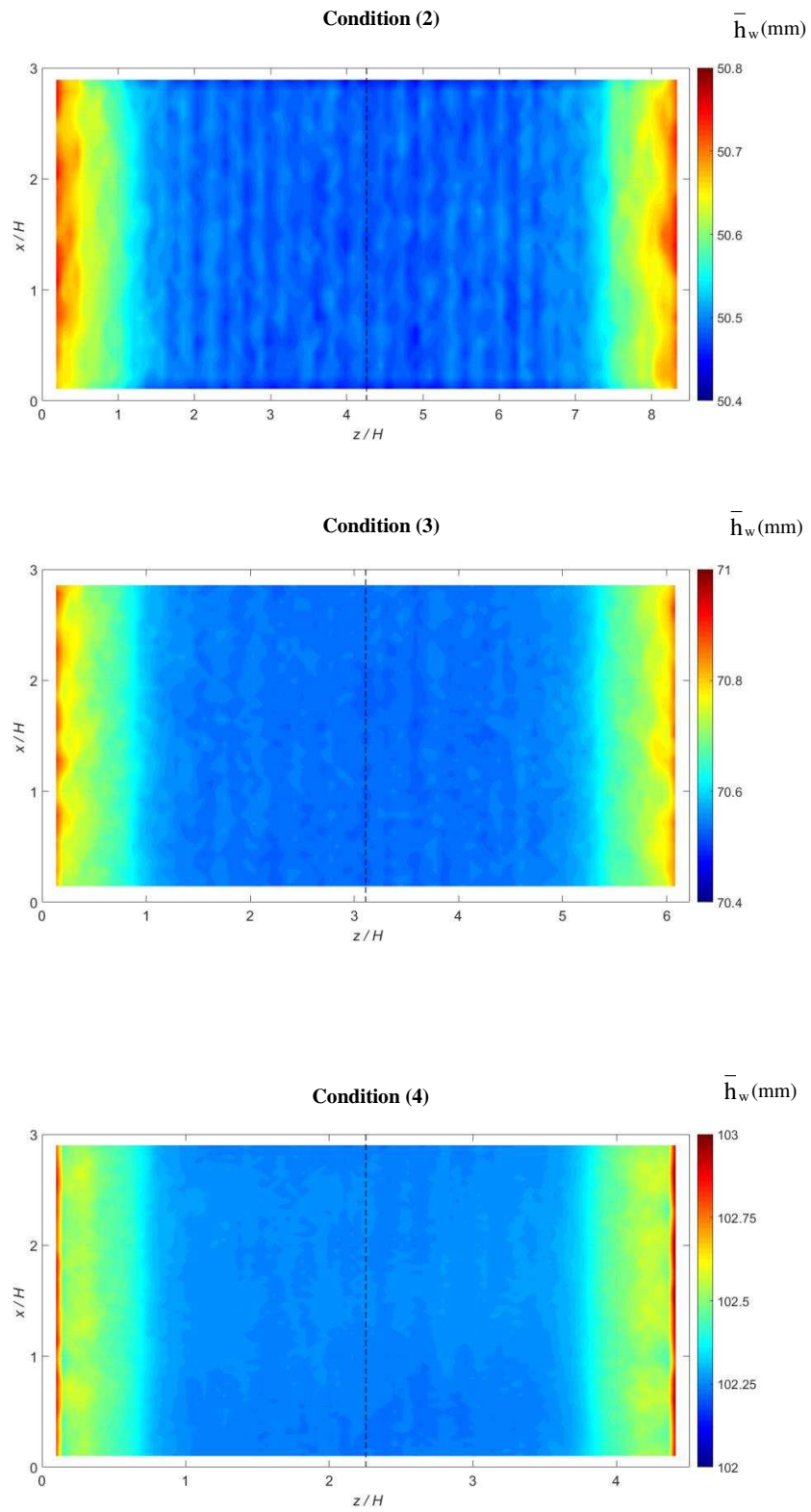$\overline{h}_w$(mm)

Fig.6. Contour plots of the computed mean free surface elevations for the four flow condition (dashed lines: flume centreline)

Table 2 presents a comparison of the computed mean water surface elevations along the flume centreline (along the black-dashed lines in Figure 6) with the experimental data. It reveals that the measured and predicted mean water depths are in good agreement with a maximum deviation approximately 2.0% of the uniform flow depth.

Table 2. Comparisons of measured and 3D SPH computed time averaged water surface levels for condition 1, 2, 3 and 4.

Flow condition	Measured $\overline{h}_w$ (mm)	Computed $\overline{h}_w$ (mm)	Deviation (%)
1	39.50	40.00	1.3
2	50.00	50.50	0.5
3	72.00	70.50	2.0
4	104.50	102.50	1.9

Additionally the mean water surface elevations measured by the two lateral wave probe arrays were compared with the computed data as presented in Figure 7. It shows that the experimental data collected by the two lateral arrays agree normally within 5.0%, 5.0%, 2.0% and 3.0% of the uniform flow depth for flow conditions 1, 2, 3 and 4 respectively. While the average errors between the predicted and measured data are 4.0%, 5.0%, 3.0% and 4.0% of the uniform flow depth for conditions 1, 2, 3 and 4, respectively.
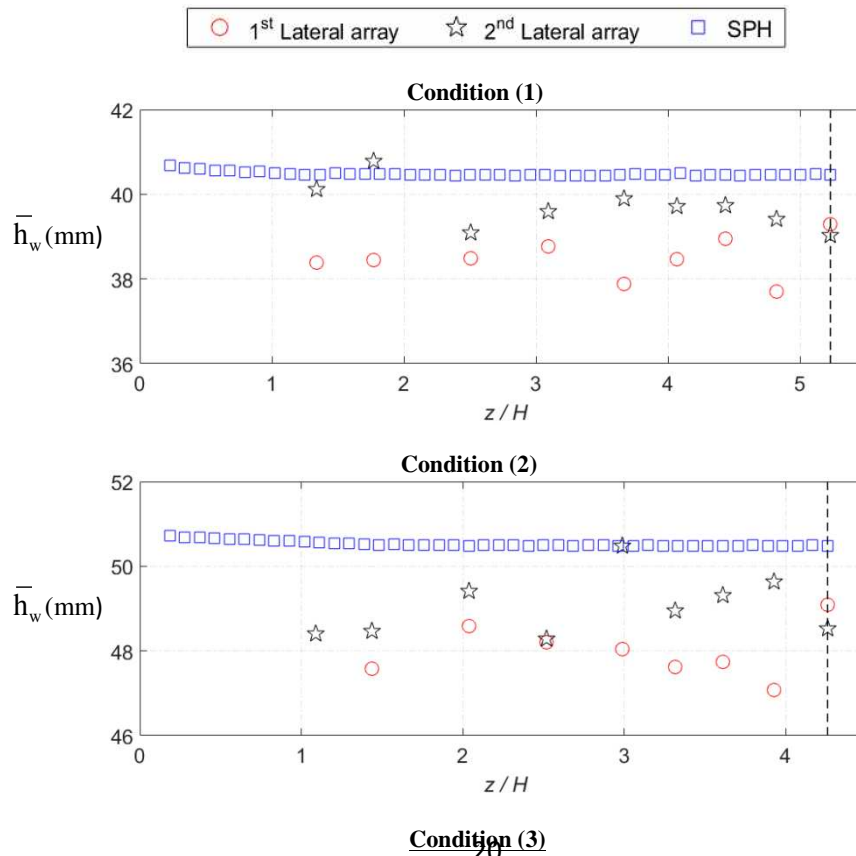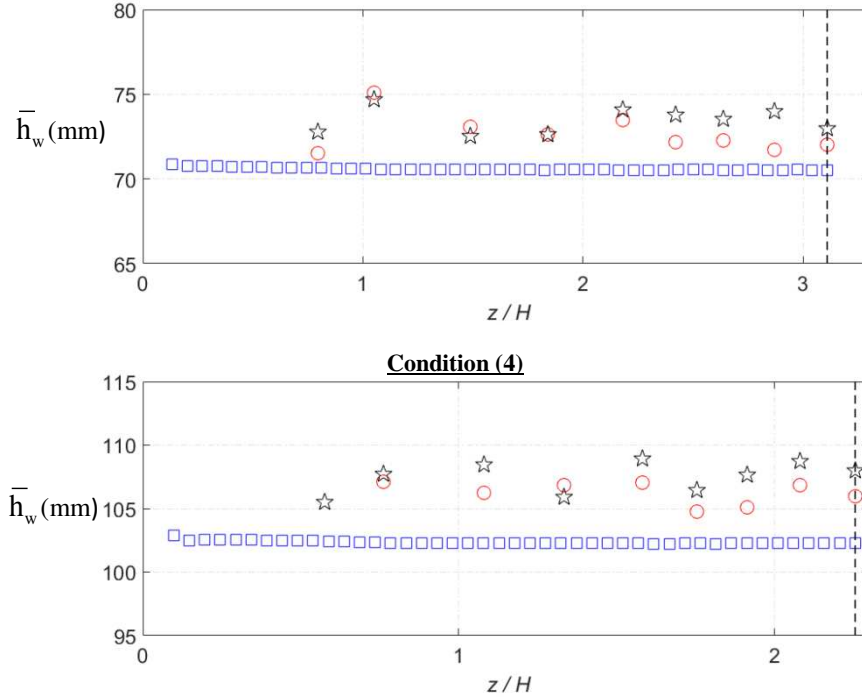
Fig.7. Comparisons of time-averaged water surface levels between experimental and 3D SPH results for flow conditions 1, 2, 3, and 4 (dashed lines: flume centreline)

5.3 Propagation of water surface pattern

This section looks at the dynamic behaviour of the water surface along the flume centreline. For each flow condition, the instantaneous water surface fluctuations h'_w at different streamwise locations were computed over t = 3.0 sec. The spatial-temporal field of the measured and computed instantaneous water surface fluctuations h'_w for the four simulated flow conditions are plotted in Figure 8 for a comparison. The black-dashed lines in Figure 8 represent the depth averaged streamwise velocity $\overline{U}$ listed in Table 1. The plots reveal that the water surface fluctuations have spatial patterns travelling with almost same orientation angles over the space and time. It can be visually judged that the slope of these patterns is very close to the depth averaged streamwise velocity $\overline{U}$. The plots also show that as the flow depth increases from condition 1 to4, the spatial period of the water surface oscillations becomes longer. All of these findings are consistent with [Fujita et al., 2011], [Horoshenkov et al., 2013] and [Nichols et al., 2016]. It should be noted that using a much more refined particle size, longer simulation time and longer flume length would allow for more accurate water surface patterns to be simulated.
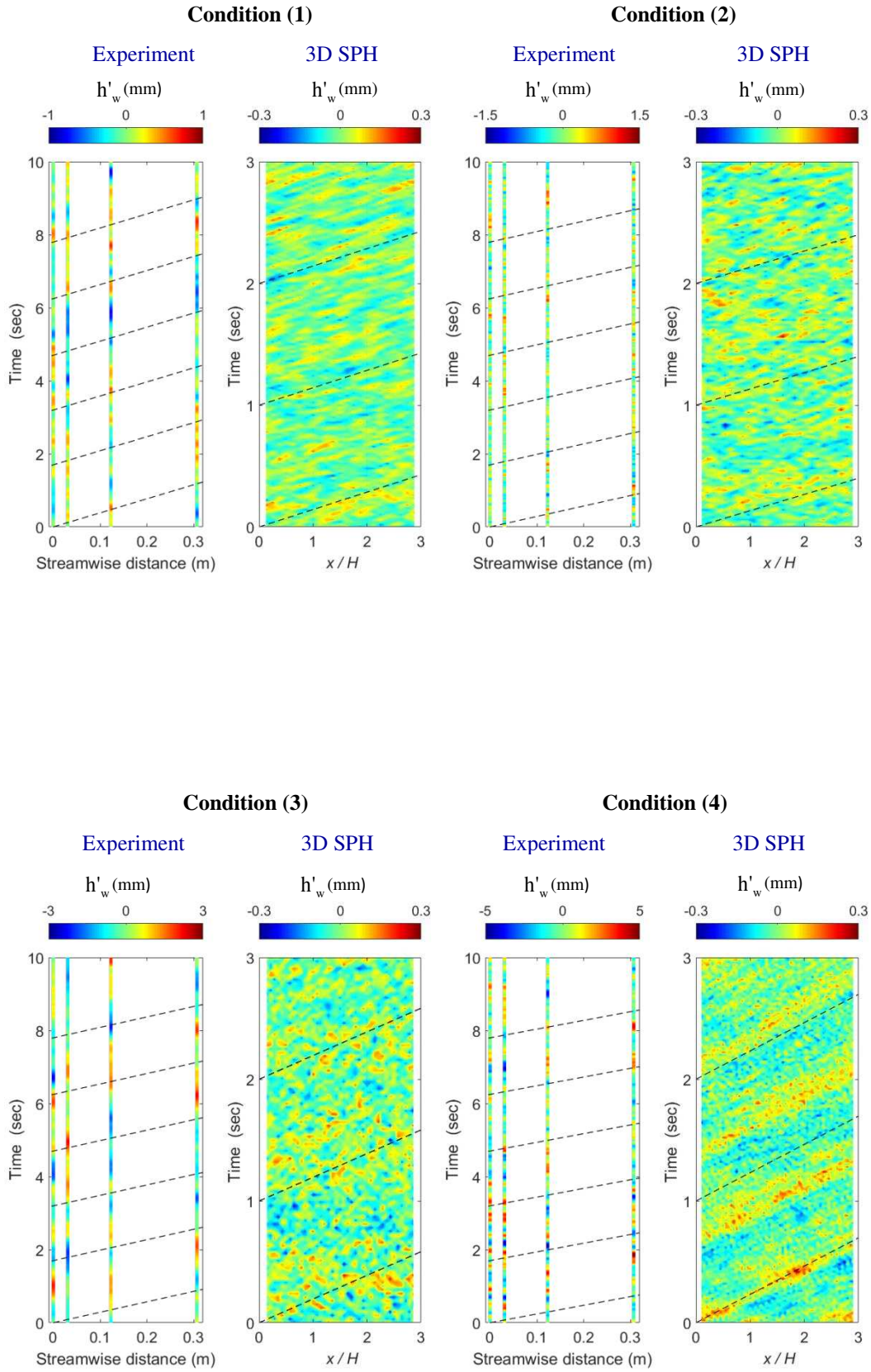
21

Fig.8. Comparisons of water surface dynamic patterns between experimental data and 3D SPH results for flow conditions 1, 2, 3 and 4 in Table 1

22

5.4 Cross correlation analysis of the free surface fluctuations

This section aims to estimate the advection speed of the computed water surface fluctuations using the cross correlation analysis. In this case, the computed free surface fluctuations along the flume centreline were cross-correlated following [Gabreil et al., 2018]in order to obtain the extreme value (maximum or minimum). Computing this for increasing separation gives rise to the spatial correlation function. This captures the temporal and spatial behaviour of the surface dynamics, and has been shown by Horoshenkov et al. [2013] to take the form of an exponentially decaying cosine which captures the dynamic fluctuation and viscous damping of surface features. Figure 9 presents the contour plots of the computed space-time correlation function for the flow condition 1, 2, 3 and 4. It can be seen that the extreme value has a unity at time lag $\tau_1 = 0$ and at spatial lag $x_1 = 0$, then it becomes smaller as both time lag and the spatial lag increase. Now, it is possible to estimate the advection speed of the water surface as $U_{wave} = x_1 / \tau_1$. It can be seen that the advection speed of the water surface (the white-dashed lines in Figure 9) is slightly less than the depth averaged velocity (the black-dashed lines in Figure 9) for the four flow conditions. The maximum deviation between the two velocities was observed in conditions 1 and 2 and it stays below 16%. Figure 10 presents a comparison of the experimental and numerical temporal cross-correlation functions against the normalized spatial lag x_1 / H for the four flow conditions. The experiment data were obtained by cross correlating the first three streamwise probes SP1 ~ SP3 giving a number of four unique pairs. While, the SPH data are the extreme values that are located along the white-dashed lines in Figure 9. In general though, the computed cross correlation function shows exponential decay in water surface pattern for the four flow conditions. A weak oscillatory component was observed for flow condition 1 and 2 (shallower) showing behaviour similar to their experiments. For conditions 3 and 4, the behaviour of the computed cross correlation function does not fluctuate as observed in the experiments. This is probably due to that the particle size used in these two deeper conditions which is around 65% bigger than the particle size used for the shallower conditions. This indicates that the ability of the SPH model to simulate spatial patterns is dependent on the vertical resolution of the water surface predictions.

Condition (1)

Cross-correlation R (-)

Condition (2)

Cross-correlation R (-)

Condition (3)

Cross-correlation R (-)
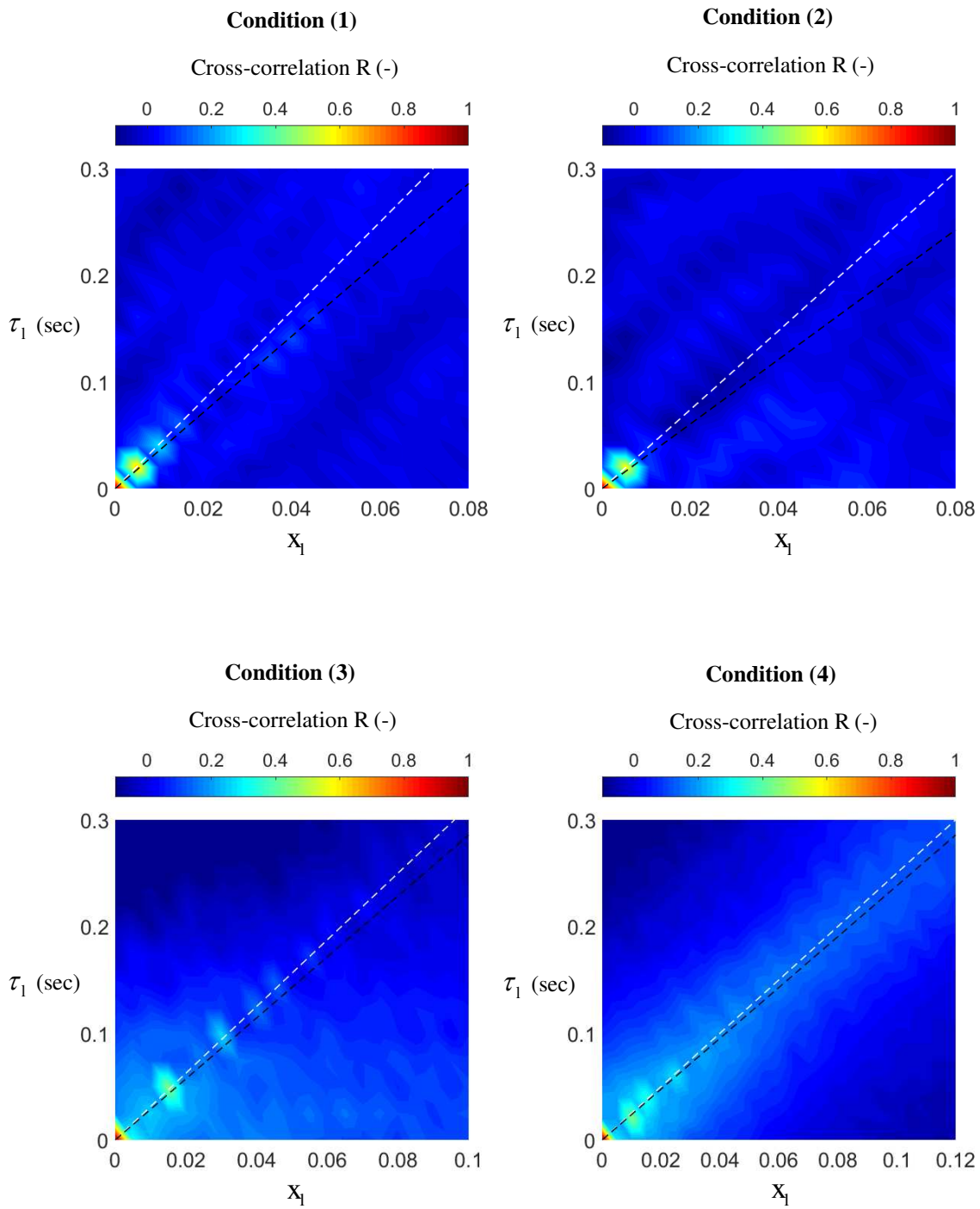

Condition (4)

Cross-correlation R (-)

Fig.9. Space-time correlation functions of the computed water surface fluctuations for flow conditions 1, 2, 3 and 4.
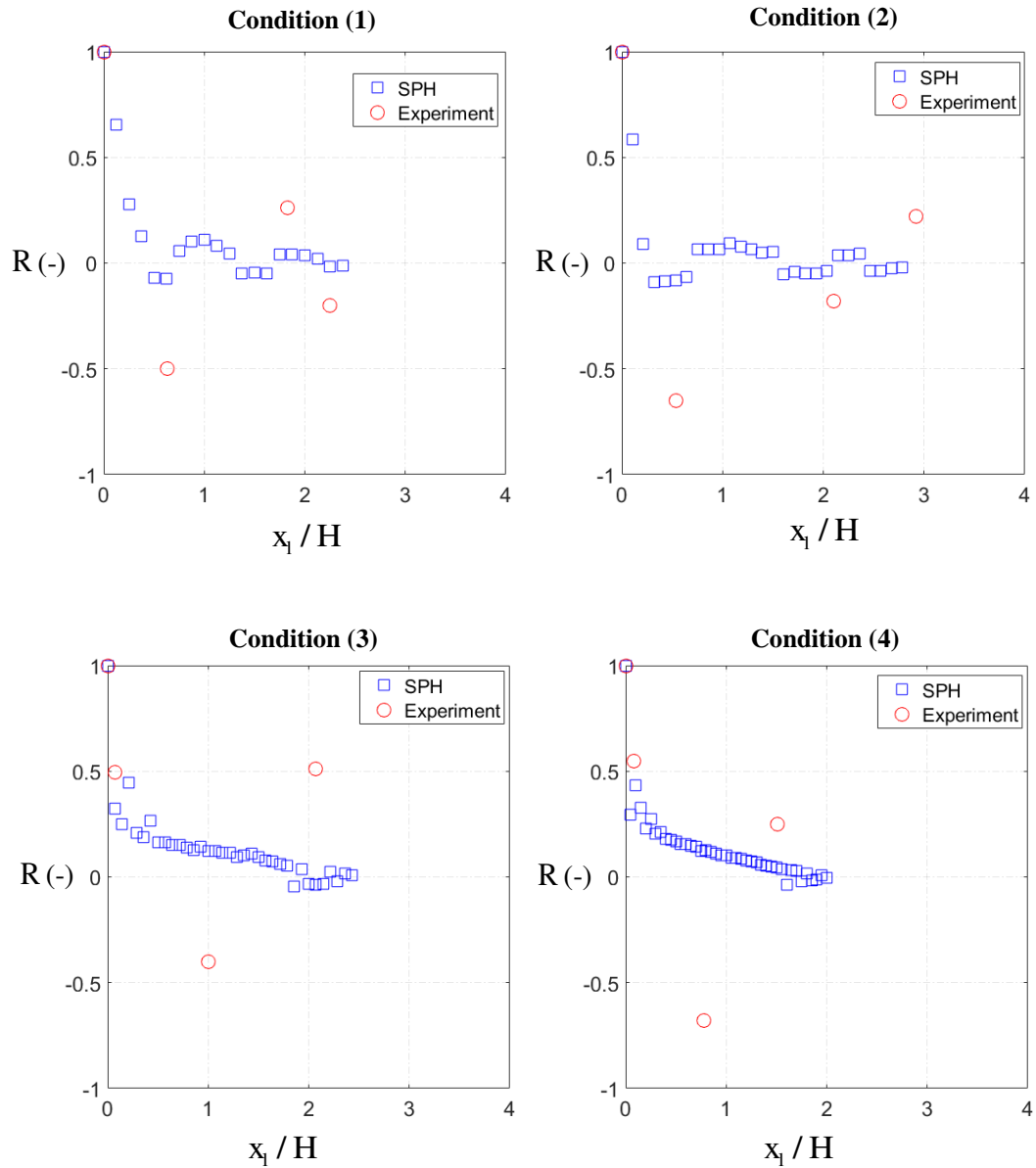
Fig.10. Experimental and numerical SPH temporal cross-correlations for flow conditions 1, 2, 3 and 4.

5.5 Correlation function of the underlying vertical flow velocity

In the previous section, it has been shown that the proposed 3D SPH model can initially simulate the free surface behaviour which was found to be closely related to the underlying main flow velocity. This section applies the spatial correlation function to the computed vertical velocity along the flume centreline and throughout the flow depth. The implementation of this technique was similar to that used in the 2D model [Gabreil et al., 2018]. The spatial correlation function of the computed vertical velocity fluctuation is presented in Figure 11 for condition 1, 2, 3 and 4.
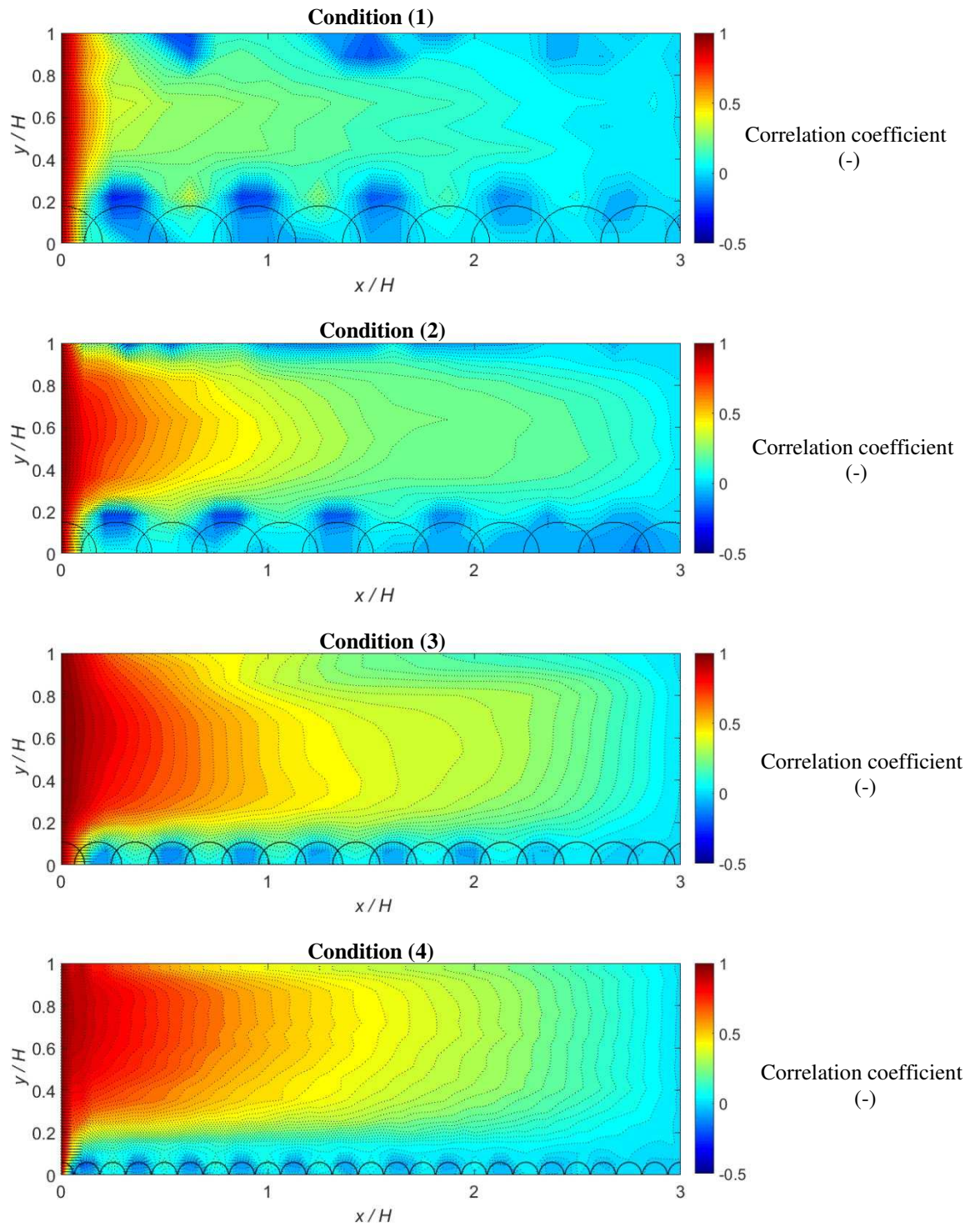
Fig.11.Computed spatial correlation function of the vertical velocity fluctuation over the flow
depth for flow conditions 1, 2, 3 and 4.

It is apparent that the influence of the bed roughness which causes the spatial correlation plots to bulge upwards. In the middle region of the flow, the spatial correlation function declines linearly such that it reaches zero correlation at shorter distance of x/H as the flow depth becomes shallower. The spatial correlation function at the free surface exhibits an oscillatory component for condition 1 and 2 (shallower). On the other hand, the correlation functions at the free surface for condition 3 and 4 (deeper) show almost linear decay. These behaviours are in reasonable agreement with those observed in the free surface (see Figure 10). The deepest zero correlation at the free surface which determines the influential depth, reaches approximately $y/H = 0.84$ for flow condition 1.

6. Conclusions

This paper proposed a 3D SPH model used to investigate its potential in simulating turbulent free surface flow over rough bed. The numerical program is based on the open source code 3DSPHysics (http://www.sphysics.org). Improvements were made on the turbulence modelling, rough bed and smooth sidewalls treatments within the code. A modified sub-particle-scale (SPS) eddy viscosity model is proposed to address the 3D turbulence effect and drag force equations in the streamwise, vertical and lateral directions were included into the momentum equations to account for the effect of rough bed and smooth sidewalls.

To validate the numerical model, experimental measurements of free surface elevations were carried out for a range of steady uniform flow conditions which cover a range of Froude Numbers. In the experiment, the temporal changes in the water surface elevations were measured using the conductance wave probe technique for all flow conditions listed in Table 1. These measurements were taken in different streamwise locations at the flume centreline and at two different lateral locations. It has been found that the probability density function (PDF) of the instantaneous water surface elevations closely follow the Gaussian distribution. The standard deviation of the water surface was found to increase as the flow becomes deeper.

The comparison between the measured and predicted mean water depths shows a good agreement with a maximum square error of 2.0%. This indicates that the developed combination of the bed and sidewall roughness provides almost the correct water depth. The cross correlation analysis has shown that both the measured and computed free surface fluctuations exhibit an oscillatory component for the shallower flow conditions. For the deeper flow conditions, the model was not able to show this behaviour. This was attributed to some numerical parameters such as computational particle size or speed of sound used in this model. The computational particle size used for deeper flow conditions was 65% bigger than the size used for shallower flow conditions. This has perhaps influenced the accuracy in simulating their water surface behaviour. The maximum error between the estimated celerity of the free surface pattern and the depth averaged velocity was found to be approximately

16.0%. The computed spatial correlation of the vertical velocity at the flume centreline has also revealed that the free surface has an influence on the sub surface vertical velocity experienced down to approximately $y/H = 0.84$. All of these numerical findings provide evidence that SPH model has the capability in simulating such flows if a suitable SPH particle size is selected.

By comparing with the previous 2D simulations [Gabreil et al., 2018], it was found that the 2D model was not able to show the change in the water surface standard deviation for the different flow conditions. Therefore, it is recommended that water surface dynamic behaviour should be studied using the 3D model since it provides results that are more consistent with the experimental observations.

The dynamic behaviour of the free surface patterns have been simulated successfully by the proposed 3D model. However, the model was not able to predict larger free surface fluctuations. This was attributed to many reasons such as the value of speed of sound and the spatial resolution used in this model. Since similar density filter and particle size were used in both models for condition 1 and 2, this would suggest that the sound speed has an influence on the standard deviation. Also the particle size used in both models is about four times larger than the measured standard deviation of water surface, which may suggest that the magnitude of water surface fluctuation was underestimated. Therefore, it is recommended to check the model accuracy in predicting larger fluctuations for bigger speed of sounds and smaller particle size. It was not possible to examine the influence of these two parameters at present as they lead to huge computational cost.

References

Cleary, P. W. & Prakash, M. [2004]. Discrete-element modelling and smoothed particle hydrodynamics: potential in the environmental sciences, Philosophical Transactions of the Royal Society A – Mathematical Physical and Engineering Sciences, 362(1822), 2003-2030.

Cooper, J. R., Tait, S. J. &Horoshenkov, K. V. [2006]. Determining hydraulic resistance in gravel-bed rivers from the dynamics of their water surfaces, Earth Surface Processes and Landforms, 31, 1839-1848.

Czernuszenko, W. &Rylov, A.A. [2000]. A generalisation of Prandtl's model for 3D open channel flows, Journal of Hydraulic Research, 38(3), 173–180.

Dabiri, D. [2003]. On the interaction of a vertical shear layer with a free surface, J. Fluid Mech., 480, 217–232.

Džebo, E., Žagar, D., Krzyk, M., Četina, M. &Petkovšek, G. [2014] Different ways of defining wall shear in smoothed particle hydrodynamics simulations of a dam-break wave, Journal of Hydraulic Research, 52, 453–464.

Dalrymple, R. A. & Knio, O. [2001]. SPH modelling of water waves, Proc. Coastal Dynamics, ASCE, 779–787, Lund, Sweden.

Farhadi, A., Ershadi, H., Emdad, H. & Rad, E. G. [2016].Comparative study on the accuracy of solitary wave generations in an ISPH-based numerical wave flume, Applied Ocean Res., 54, 115–136.

Fedderico, I., Marrone, S., Colagrossi, A., Aristodemo, F., Antuono, M. (2012), Simulating 2D open-channel flows through an SPH model, European Journal of Mechanics, 34, 35–46.

Fujita, I., Furutani, Y. &Okanishi, T. [2011]. Advection features of water surface profile in turbulent open-channel flow with hemisphere roughness elements, Vis. Mech Proc., 1(4), doi:10.1615/VisMechProc.v1.i3.70.

Gabreil, E. [2017]"Application of Smoothed Particle Hydrodynamics Modelling to Turbulent Open Channel Flows over Rough Beds," PhD Thesis, University of Sheffield, Sheffield, UK.

Gabreil, E., Tait, S. J., Shao, S. & Nichols, A. [2018].SPHysics simulation of laboratory shallow free surface turbulent flows over a rough bed, J. Hydr. Res., DOI: 10.1080/00221686.2017.1410732.

Gingold, R. A. &Monaghan J. J. [1977].Smoothed particle hydrodynamics: theory and application to non-spherical stars, Mon. Not. R. Astron. Soc., 181, 375–389.

Gotoh, H. & Sakai, T. [1999].Lagrangian simulation of breaking waves using particle method, J. Coast. Eng., 41(3&4), 303–326.

Gotoh, H., Shibahara, T. & Sakai, T. [2001]. Sub-Particle-Scale turbulence model for the MPS method — Lagrangian flow model for hydraulic engineering,J. Comp. Fluid Dyn., 9(4), 339–347.

Horoshenkov, K. V., Nichols, A., Tait, S. J. &Maximov, G. A. [2013].The pattern of surface waves in a shallow free surface flow, J. Geophysical Res, Earth Surface, 118(3), 1864–1876.

Kazemi E, Nichols A, Tait S, Shao S [2017]. SPH modelling of depth limited turbulent open channel flows over rough boundaries. International Journal for Numerical Methods in Fluid, 83(1), 3–27.

Khayyer, A. &Gotoh, H. [2010]. On particle-based simulation of a dam break over a wet bed, J. Hydraul. Res., 48 (2), 238–249.

Koshizuka, S., Nobe, A., Oka, Y. [1998]. Numerical analysis of breaking waves using the moving particle semi-implicit method, Int. J. Numer. Meth. Fluids, 26(7), 751–769.

Krynkin, A., Horoshenkov, K. V., Nichols, A. & Tait, S. J. [2014].A non-invasive acoustical method to measure the mean roughness height of the free surface of a turbulent shallow water flow, Review of Scientific Instruments, 85(11), 114902.

Kumar, S., Gupta, R. and Banerjee, S. [1998].An experimental investigation of the characteristics of free-surface turbulence in channel flow, J. Phys. Fluids, 10(2), 437–456.

Lee, E.-S., Moulinec, C., Xu, R., Violeau, D., Laurence, D. &Stansby, P. [2008]. Comparisons of weakly compressible and truly incompressible algorithms for the SPH mesh free particle method, J. Comp. Phys., 227, 8417–8436.

Li, S. & Liu, W. [2004].Meshfree Particle Methods, New York: Springer.

Lo EYM & Shao SD [2002]. Simulation of near–shore solitary wave mechanics by an incompressible SPH method. APPLIED OCEAN REFEARCH, 24(5), 275–286.

Mathieu, J. & Scott, J. [2000]. An Introduction to Turbulent Flow, Cambridge: Cambridge University Press.

Meister, M., Burger, G. & Rauch, R. [2014]. On the Reynolds number sensitivity of smoothed particle hydrodynamics, J. Hydr. Res., 52(6), 824–835.

Monaghan, J. J. [1992]. Smoothed Particle Hydrodynamics, Annu. Rev. Astrophys, 30, 543–574.

Nakagawa, H., Nezu, I. & Ueda, H. [1975].Turbulence in open channel flow over smooth and rough beds, Proc. Japan Soc. Civil Engrs., 241, 155–168.

Nichols, A., Tait, S. &Horoshenkov, K., [2010]. Remote Characterisation of Shallow Flows from the 'Fingerprint' of the Free Surface, Yorkshire: Yorkshire Water Department.

Nichols,A[2014] "Free Surface DynamicinShallow Turbulent Flows,"PhD Thesis, The University of Bradford, Bradford, UK.

Nichols, A., Tait, S. J., Horoshenkov, K. V. & Shepherd, S. J. [2016].A model of the free surface dynamics of shallow turbulent flows, Journal of Hydraulic Research, 54(5), 516–526.

Onate, E., Idelsohn, S., Zienkiewicz, O. C., Taylor, R. L. [1996].A Finite Point method in computational mechanics, Applications to Convective Transport and Fluid Flow, Int. J. Numer. Methods Engrg., 39, 3839–3866.

Petkovšek, G., Džebo, E., Cetina, M., Žagar, D., [2010]. Application of non discrete boundaries with friction to smoothed particle hydrodynamics. J. Mech. Eng. 56(5), 307–315.

Roubtsova, V. &Kahawita, R. [2006]. The SPH technique applied to free surface flows, Computers and Fluids, 35(10), 1359-1371.

Savelsberg, R. & van de Water, W. [2006]. Measurement of the gradient field of a turbulent free surface, J. Exp in Fluids., 41, 629–640.

Savelsberg, R. & van de Water, W. [2009].Experiments on free-surface turbulence, J. Fluid Mech., 619, 95–125.

Shakibaeinia, A. & Jin, Y. C. [2010].A weakly compressible MPS method for modeling of open-boundary free surface flow, Int. J. Numer. Methods Fluids, 63(10), 1208–1232.

Shao SD & Lo EYM [2003]. Incompressible SPH method for simulating Newtonian and non–Newtonian flows with a free surface. ADVANCES IN WATER RESOURCES, 26(7), 787–800.

Smolentsev, S. and Miraghaie, R. [2005].Study of a free surface in open channel water flow in the regime from "weak" to "strong" turbulence, Int. J. Multiphase Flow, 31, 921–939.

Tan, S. K., Cheng, N-S., Xie, Y. & Shao, S. [2015].Incompressible SPH simulation of open channel flow over smooth bed, Journal of Hydro-Environment Research, 9(3), 340–353.

Violeau, D. [2012]. Fluid Mechanics and the SPH Method: Theory and Applications, Oxford: Oxford University Press.

Yagawa, G. & Yamada, T. [1996]. Free mesh method: a new meshless finite element method, Comput. Mech, 8, 383–386.